

# Additive Manufacturing of Nanostructures That Are Delicate, Complex, and Smaller than Ever

Andrew J. Gross and Katia Bertoldi\*

**Additive manufacturing with two-photon polymerization (TPP) has opened new opportunities for the rapid fabrication of 3D structures with sub-micrometer resolution, but there are still many fabrication constraints associated with this technique. This study details a postprocessing method utilizing oxygen-plasma etching to increase the capabilities of TPP. Underutilized precision in the typical fabrication process allows this subtractive technique to dramatically reduce the minimum achievable feature size. Moreover, since the postprocessing occurs in a dry environment, high aspect ratio features that cannot survive the typical fabrication route can also be achieved. Finally, it is shown that the technique also provides a pathway to realize structures that otherwise are too delicate to be fabricated with TPP, as it enables to introduce temporary support material that can be removed with the plasma. As such, the proposed approach grants access to a massively expanded design domain, providing new capabilities that are long sought in many fields, including optics, biology, robotics, and solid mechanics.**

Two-photon polymerization (TPP) is enabling fabrication of structures with a combination of small scale resolution and geometric freedom beyond previous capabilities.<sup>[1]</sup> As such, it has become a popular fabrication technique to study physical systems and phenomena across many disciplines where miniaturization and effects on the nano and microscales are relevant, including optics,<sup>[2–7]</sup> biology,<sup>[8–10]</sup> bioengineering,<sup>[11–13]</sup> robotics,<sup>[14–16]</sup> and solid mechanics.<sup>[17–20]</sup> Yet, fabrication with TPP in the most commonly used configuration—where the objective lens of the microscope is in direct contact with a liquid resist—still poses critical design constraints. For example, studies of microlattices have noted that these structure are too delicate to be fabricated when their struts are more than 17.5 times longer than

their diameter.<sup>[21]</sup> Additionally, it has been observed that the resolution of the technique sets a lower bound for the strut diameters to be around 1  $\mu\text{m}$ .<sup>[19]</sup>

To overcome these limitations, a number of variations of TPP have been explored.<sup>[22–28]</sup> Out of these, the stimulated emission depletion (STED) approach is particularly promising and has demonstrated the smallest feature sizes, allowing for the fabrication of freestanding 3D structures with strut cross-sectional dimensions as small as 120  $\times$  170 nm<sup>[29]</sup> with resolutions of 175 and 375 nm in the sense of Abbe and Sparrow, respectively.<sup>[30]</sup> However, the STED approach requires complexity in setup that is currently out of reach to most researchers and has only been demonstrated using the conventional oil-immersion configuration, which is decreasing in popularity and limits structures to be less than 100  $\mu\text{m}$  in height. Alternative approaches to enhancing the capabilities of TPP through subtractive methods have also recently been proposed. In particular, new photoresist chemistries that allow for chemically selective removal of one type of photoresist from another through a wet process have been developed, enabling the fabrication of more delicate structures.<sup>[31–33]</sup> Moreover, the use of oxygen-plasma etching and pyrolysis has been recently proposed to reduce the dimensions of structures fabricated with TPP,<sup>[34]</sup> demonstrating that the minor diameter of elliptical struts in a wire-like structure can be reduced to around 25 nm. However, the use of oxygen-plasma etching for fabrication has been confined to the case of a structure where the local geometry is arbitrarily determined by the spheroidal voxel shape that is natural to TPP.<sup>[34]</sup>

As a result, no control over the local geometry that is achieved after etching or ability to leverage the geometric freedom that is natural with additive manufacturing has been realized.

Here, inspired by recent progress using subtractive modifications, we propose two new fabrication concepts that make use of both TPP and oxygen-plasma etching as a subtractive operation: i) the use of high precision shape control in the initial geometry to achieve smaller feature sizes after subtractive postprocessing; ii) the use of sacrificial support material that can be removed through dry subtractive postprocessing to enable the fabrication of structures that are otherwise too delicate to be realized. In particular, we leverage the underutilized precision of the piezo microscope stages and galvo scanners that are typically used to raster the TPP voxel to attain feature sizes after etching that are substantially smaller than the voxel size in TPP. Moreover, we

Dr. A. J. Gross, Prof. K. Bertoldi  
John A. Paulson School of Engineering and Applied Sciences  
Harvard University  
Cambridge, MA 02138, USA  
E-mail: bertoldi@seas.harvard.edu  
Prof. K. Bertoldi  
Kavli Institute  
Harvard University  
Cambridge, MA 02138, USA  
Prof. K. Bertoldi  
Wyss Institute for Biologically Inspired Engineering  
Harvard University  
Cambridge, MA 02138, USA

 The ORCID identification number(s) for the author(s) of this article can be found under <https://doi.org/10.1002/smll.201902370>.

DOI: 10.1002/smll.201902370

show that microlattice structures can be used as a temporary support material to enable the fabrication of delicate and complex primary structures, which can also reach final feature sizes that are smaller than can be achieved with the typical approach to TPP. These simple dry postprocessing methods can be applied to virtually all TPP variants to substantially improve the minimum achievable size and increase the feasible design domain to enable the fabrication of very delicate and complex structures. In this article, we apply them to several structures fabricated with TPP operated in the most commonly used configuration (often referred to as dip in laser lithography or DiLL<sup>[35]</sup>) and demonstrate that they enable realization of systems that would be exceedingly difficult or unfeasible with any other approach.

We start by investigating the ability of O<sub>2</sub> plasma to reduce the dimensional features of a microlattice structure. To this end, we use TPP (Photonic Professional GT, Nanoscribe GmbH) to fabricate an octahedral microlattice with a straight line laser trajectory, subsequently referred to as Lattice 1. The struts in Lattice 1 are  $L = 7.0 \mu\text{m}$  long and have a cross-sectional shape that is elliptical, with some variability in cross-sectional dimensions that is correlated to the strut orientation. Several representative struts were measured to have a minor diameter  $b_0 = 380 \pm 7 \text{ nm}$  and an aspect ratio  $a_0/b_0 = 2.3 \pm 0.05$  ( $a_0$  being the major diameter) directly after fabrication. These representative struts were monitored throughout successive exposure to O<sub>2</sub> plasma. As shown in Figure 1a, we find that isotropic surface etching from an exposure time  $t = 11 \text{ min}$  to oxygen-plasma pushes Lattice 1 to the brink of collapse and further etching results in nearly complete removal (see Figure S1 in the Supporting Information for an image of a lattice after removal and images of a similar partially collapsed lattice at  $t = 11 \text{ min}$ ). After  $t = 11 \text{ min}$  of etching, the cross-section for representative struts are measured to have reduced minor diameters  $b = 68 \pm 6 \text{ nm}$  with increased aspect ratios  $a/b = 5.9 \pm 0.5$ . Additionally, it is observed that the struts on the exterior of the structure are etched to slightly smaller dimensions than those in the interior, due to greater accessibility to the plasma (see Figure S2 in the Supporting Information). As a result, the smallest strut realized from this specimen is

located on its top surface and contained segments with a minor diameter  $b$  as small as 19 nm (see Figure 1b). However, fluctuations in the dimensions of any one strut due to slight irregularities during polymerization cause other segments of this smallest strut to have  $b > 34 \text{ nm}$  (note that even greater fluctuations are found for the major diameter, with  $75 < a < 350 \text{ nm}$ ).

To overcome the limitations posed by the shape and slight fluctuations in size of the native voxel, we introduce a slightly more sophisticated laser trajectory that results in better control of the cross-sectional dimensions of the struts in the microlattice. Specifically, the trajectory follows elliptical helices to expose inclined features, and a multiple pass, linear trajectory to expose features that are perpendicular to the optical axis. The structure shown in Figure 1c, subsequently referred to as Lattice 2, is fabricated with such a laser trajectory, the elliptical helices set to have a pitch of 110 nm for inclined struts, and horizontal struts fabricated with 20 closely spaced passes  $\approx 110 \text{ nm}$  apart. It should also be noted that the struts on the exterior of Lattice 2 were fabricated with a laser power 8% higher than those on the interior to compensate for their greater accessibility to the plasma. Finally, orientation dependence of the strut size was tuned not to exceed 110 nm after etching. The precise trajectory used to create Lattice 2 is included in the Supporting Information, but no matter the specifics of the laser trajectory, two key characteristics for the struts in the resulting microlattice were targeted: i) a nearly equiaxed cross-section (i.e.,  $a_0/b_0 \approx 1$ ) and ii) geometric precision of the cross-section at a scale below the voxel size of the TPP technique utilized. Both of these characteristics are quite commonplace, the former being a common design choice and the latter being a consequence of both the stability of the voxel size (which is not guaranteed for all exposure conditions) and the high precision capability of piezo microscope stages and galvo scanning systems. Directly after fabrication, exterior struts that are inclined to the optical axis are measured to be  $4.2 \mu\text{m}$  in length and have cross-sectional dimensions  $a_0 = 1579 \pm 17 \sim b_0 = 1505 \pm 17 \text{ nm}$ . Importantly, etching of Lattice 2 results in struts with reduced dimensions that retain the equiaxed cross-section, allowing for

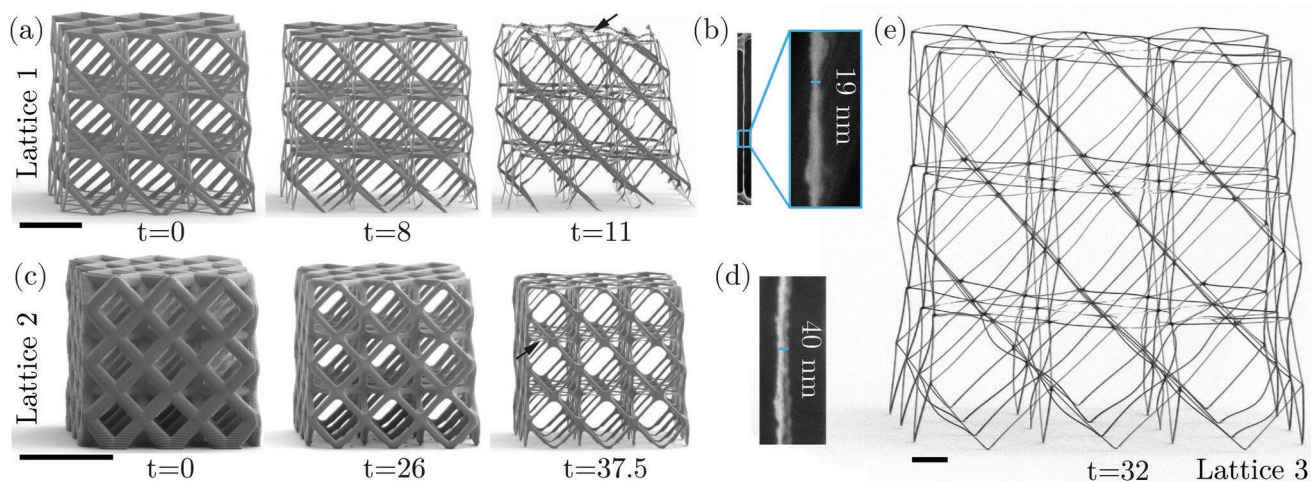


**Figure 1.** a) Progressive etching of Lattice 1, comprising elliptical struts. The arrow indicates the strut shown in (b) with high magnification. c) Progressive etching of Lattice 2, comprising equiaxed struts. The arrow indicates the strut shown in (d) with high magnification. e) Lattice 3 at the final stage of etching. All scale bars are  $10 \mu\text{m}$  and all etching times  $t$  are reported in minutes.

substantial reduction in all cross-sectional dimensions. After 37.5 min of exposure to O<sub>2</sub> plasma, the smallest struts reduce to have  $a \approx b \approx 40$  nm (see Figure 1d). Limitations to further reductions in strut size include fluctuations in strut size as initially fabricated and sensitivity of the struts to the beam of the scanning electron microscope used for observation. Nonetheless, the size achieved with the current technique is 25 times smaller than struts fabricated with typical TPP,<sup>[19]</sup> 4 times smaller than the smallest 3D structure fabricated with STED enhanced TPP,<sup>[29]</sup> and even below the size of the smallest 2D pattern reported using the STED approach.<sup>[36]</sup> At this point it should be noted that our postprocessing approach does not allow for a reduction in spacing between neighboring features as STED does. However, it can also be applied to structures fabricated with STED, so that the two techniques should be seen as complimentary to one another rather than in competition.

In addition to the substantial reduction in feature size achieved with O<sub>2</sub>-plasma etching, the proposed approach also provides a pathway to modify structures as a means to achieve geometric forms that are otherwise unable to be fabricated. To demonstrate this important point, we use a laser trajectory identical to that of Lattice 2 to fabricate a microlattice with longer struts, subsequently referred to as Lattice 3. Other than the longer struts, the only change from Lattice 2 is that the laser power used to expose the exterior struts was changed to be only 5% higher than the interior struts. A characteristic set of struts in the interior of Lattice 3 are measured to have  $L = 24.9$  μm and  $a_0 = 1389 \pm 46 \sim b_0 = 1344 \pm 36$  nm. In Figure 1e, we show Lattice 3 after 32 min of plasma exposure. We find that the average strut diameter is reduced to  $a \approx b \approx 175 \pm 7$  nm, thus increasing the slenderness of the struts 8 times beyond what has been previously reported,<sup>[21]</sup> with  $L/a = 140$ . After 32 min of etching, Lattice 3 has a relative density (the fraction of solid material contained within its exterior dimensions) of  $1.7 \times 10^{-4}$ , which is 60 times less than any other material existing at a similar length scale with comparable topology (i.e., microlattices that are not hierarchical and are comprised of struts with a solid cross-section).<sup>[21]</sup> Furthermore, no perceivable distortion occurs during the plasma exposure; even the few struts adjacent to the substrate that bent slightly during development do not distort during material removal.

While up to this point we focused on the geometric modifications that can be applied to a structure with the use of etching, we are inspired by the ubiquity of support material in desktop 3D printing to investigate if microlattices can be used as temporary support material to enable the fabrication of structures that are otherwise too delicate to be realized with TPP. To gain insight in the factors that govern microlattice removal, we begin by focusing on the three lattices shown in Figure 1 and monitor the major and minor diameters  $a$  and  $b$  of several struts during etching. For Lattices 1 and 3 the struts monitored are in the interior of the specimen, whereas for Lattice 2 the exterior struts exposed with increased laser power are monitored, since the structure is initially too dense to observe the interior struts. The results shown in Figure 2a indicate that Lattices 2 and 3 persist in the O<sub>2</sub> plasma for more than 37.5 and 32 min, respectively, far longer than Lattice 1, which requires just over 11 min to be almost completely etched away. Such difference in the time required for complete removal of each lattice is a function of the

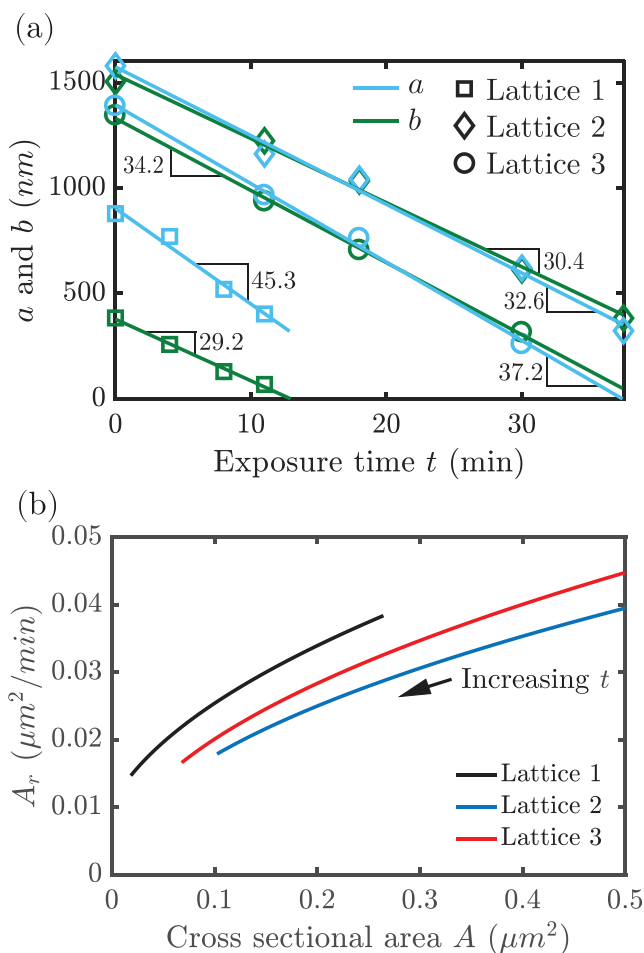


**Figure 2.** a) Experimentally measured major and minor diameters  $a$  (blue) and  $b$  (green) for Lattice 1 (square data points), Lattice 2 (diamond data points), and Lattice 3 (circular data points) during etching. Best fit lines are used to calculate the etching rates  $R_a$  and  $R_b$ , which are reported on the plot in units of nm min<sup>-1</sup>. b) Areal removal rate  $A_r$  as a function of cross-sectional area for Lattices 1, 2, and 3.

size, shape, and exposure conditions of the struts that comprise it. Moreover, the results indicate that the diameters  $a$  and  $b$  of each lattice etch at different, but constant rates,  $R_a$  and  $R_b$ . The difference between the etching rate in each direction is substantial for the elliptical struts of Lattice 1, with  $R_a$  being 55% larger than  $R_b$ . Such anisotropy in the etching rate is likely a consequence of heterogeneity in the crosslinking density in the voxel, which decreases with distance from the focal point.<sup>[23]</sup> Furthermore, anisotropy in the directional etching rates is found to be sensitive to the laser trajectory used for fabrication, with the ratio of  $R_a$  to  $R_b$  being almost 7 times higher for Lattice 1 (fabricated with a straight line laser trajectory) than for Lattices 2 and 3 (fabricated with helical laser trajectories). As a whole, our results show that the directional etching rate is inversely proportional to the exposure dose. This is most apparent when comparing the directional etching rates between struts observed in Lattices 2 and 3, where the struts in Lattice 2 (which are exposed with higher laser power than those in Lattice 3) are observed to have smaller directional etching rates than those in Lattice 3.

To further separate the effect of cross-sectional shape, size, and crosslinking density on the overall removal rate of a strut, we next estimate the rate at which material is removed from a representative cross-section as

$$A_r = C \frac{R_a + R_b}{2} \quad (1)$$

where  $C$  is the perimeter of the elliptical cross-section at etching time  $t$ , which can be calculated from the etched major and minor diameters  $a = a_0 - R_a t$  and  $b = b_0 - R_b t$  as<sup>[37]</sup>

$$C = \frac{\pi(a+b)}{2} \left( 1 + \frac{3h}{10 + \sqrt{4-3h}} \right) \quad (2)$$

with  $h = (a - b)^2 / (a + b)^2$ . In Figure 2b, we show the areal removal rate  $A_r$  (calculated using Equation (1) and the etching rates extracted from Figure 2a) as a function of cross-sectional area  $A = \pi ab$  for Lattices 1, 2, and 3. The plot reveals that, as a result of the various exposure conditions (i.e., crosslinking density) and cross-sectional shapes (i.e., surface area to volume ratio), each lattice has a different areal removal rate across the range of cross-sectional sizes. Specifically, we find at a given cross-sectional area  $A$ , the areal removal rate for Lattice 2 is  $\approx 12\%$  less than for Lattice 3. Since these two lattices have the same cross-sectional shape, this difference is completely due to the greater laser power used to expose the struts in Lattice 2. Making the same comparison between Lattice 1 and Lattice 3, we observe that the elliptical struts of Lattice 1 are removed on average 23% faster than the equiaxed ones of Lattice 3. However, in this case the difference is dominated by the effect of cross-sectional shape, as the average surface area to volume ratio is 18% larger for Lattice 1 over the considered range of cross-sectional areas. Lastly, comparison between the areal removal rates between Lattices 1 and 2 shows that Lattice 1 is removed on average 40% faster, with differences in geometry and exposure conditions contributing nearly equally to this difference. Therefore, our analysis makes it clear that both the shape of the struts and the exposure conditions affect the removal rate of a microlattice. Furthermore, they indicate that microlattices fabricated with a straight line laser trajectory to create elliptical struts with minimal exposure dose and initial size are promising candidates to serve as temporary support material, as they can be completely removed with short exposure times to  $O_2$ .

Next, to test if microlattices comprising elliptical struts with minimal exposure dose and initial size can be used as temporary support material to enable the fabrication of structures that are too delicate to otherwise be fabricated with TPP, we set out to realize an array of curved cantilever beams with length of  $190.5 \mu\text{m}$  and cross-sectional dimensions of  $19.0 \mu\text{m} \times 2.3 \mu\text{m}$ , which are supported

$50 \mu\text{m}$  above the substrate by a structurally robust abutment. To avoid steps along their length, the beams are fabricated flat and exposed with a graded laser power across their thickness to cause a prestress upon development that deforms them to their programmed curvature.<sup>[38]</sup> Although geometrically simple, we find that fabrication of this structure without the inclusion of support material leads to severe defects in the forms of uncontrolled bending during development (even though  $CO_2$  supercritical point drying is employed), and stacking errors between subsequent layers of each beam during exposure (see Figure 3a). To eliminate both of these defects, we then fabricate the beams on an octahedral microlattice (comprising struts with a length of  $L = 7.16 \pm 0.1 \mu\text{m}$  and cross-sectional dimensions  $a_0 = 1630 \pm 60 \text{ nm}$  and  $b_0 = 560 \pm 20 \text{ nm}$ ) that acts as supporting material (Figure 3b,c). Remarkably, we find that such a supporting structure both prevents their motion during exposure and stabilizes the beams during development. Finally, and most importantly, the support material can be removed with 25 min of exposure to  $O_2$  plasma, with only minor evidence of its initial presence remaining afterward (Figure 3d). Once the support material is removed, the beams are released and the prestress that was programmed during their exposure causes them to bend as intended. It should be noted that during removal of the support material, the plasma also reduces the beam thickness to  $1.3 \pm 0.1 \mu\text{m}$ . Although dimensional modification of the primary structure is unavoidable with this approach, the size reduction is often times desirable and is simple to compensate for in the initial fabrication of the primary structure.

Finally, we investigate how generally our technique of including support material can be applied to complex 3D objects with even greater delicacy at the nanoscale, and use it

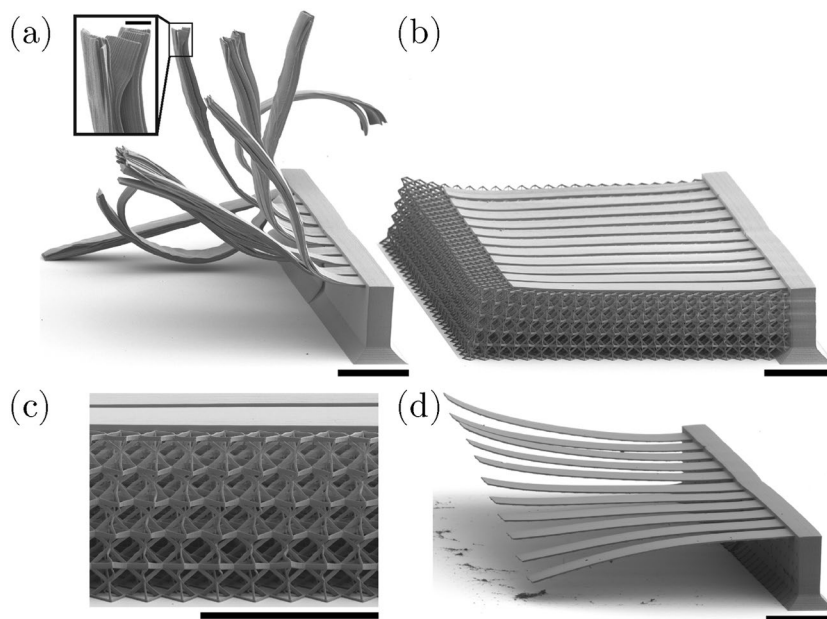


**Figure 3.** a) Fabrication errors and distortions that occur during exposure and development of a beam array with no supports. Inset shows stacking errors between subsequent layers. b) Defect free beam array supported by an octahedral microlattice. c) Magnified view of one beam resting on the bed of support material. d) Beam array after support material is removed. The curvature of each beam is achieved with a gradient in exposure through the thickness of each beam. Scale bar in the inset image is  $5 \mu\text{m}$ , all others are  $50 \mu\text{m}$ .

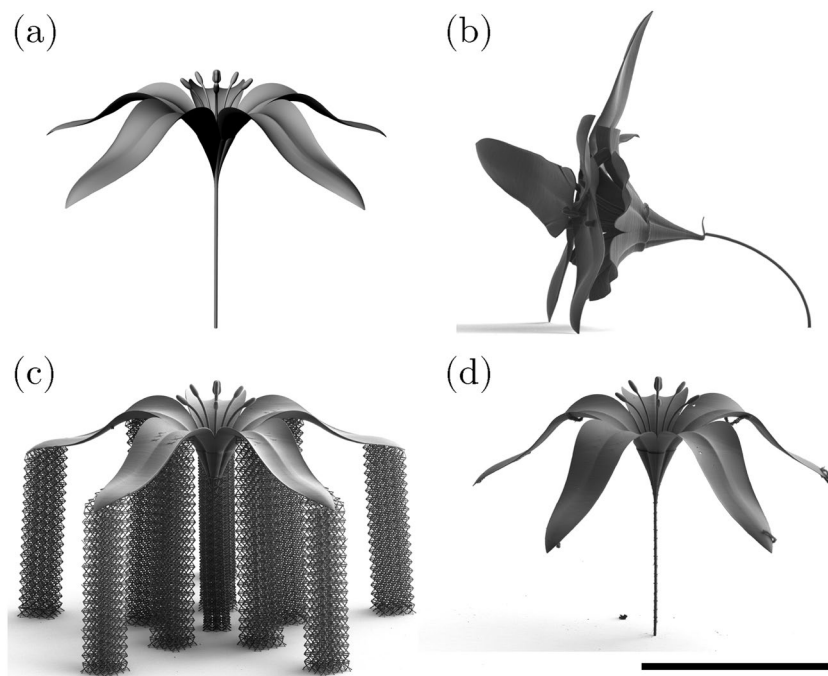


**Figure 4.** a) CAD rendering of the considered flower design. b) Fabrication errors and distortions that occur during exposure and development of the flower with no supports. c) Defect free flower supported by octahedral microlattices. d) Flower after support material is removed. All images are at the same scale and the scale bar is 200  $\mu\text{m}$ .

to fabricate a flower comprising several exceedingly thin and slender elements (see the CAD design in **Figure 4a**). Target dimensions of the flower are: 3  $\mu\text{m}$  diameter stem, 295  $\mu\text{m}$  overall height, and petals that have an arc length of 250  $\mu\text{m}$  with a thickness of 0.5  $\mu\text{m}$ . As expected, when the flower is constructed without the use of support material, major defects emerge: the stem tips over during development and critical point drying and the petals are misplaced during exposure (see **Figure 4b**). The gross misplacement of the petals is a consequence of the large lateral dimensions of the flower, which requires that the stage be moved during exposure. These stage movements induce extensive flow in the resist, causing large deformation of the delicate structure after which precise positioning of the petals on the stem cannot be restored (see **Video S1** in the Supporting Information). To stabilize the flower during exposure and development, an octahedral microlattice (comprising struts with a length of  $L = 7.16 \pm 0.1 \mu\text{m}$  and cross-sectional dimensions  $a_0 = 950 \pm 50 \text{ nm}$  and  $b_0 = 380 \pm 20 \text{ nm}$ ) is used for supporting material as shown in **Figure 4c**. Support of the stem is achieved by encasing it in a microlattice tower, whereas each petals is stabilized by two tower-like supporting structures that are fabricated after the stem and its support are complete, but before the petals are exposed (see **Video S2** in the Supporting Information). Lesser support of the petals, with only one tower located at their tips, was found to be insufficient to avoid motion of the petals during exposure, but adequate to stabilize them during development (see **Video S3** and **Figure S3** in the Supporting Information). It should also be noted that the fabrication of the stem requires the ability to quickly switch between depositing support and primary structure.

This enables the slender stem to be built in mechanically robust freestanding segments, each of which are encased in a supporting microlattice before proceeding to the next segment. This sequential strategy is superior to continuous exposure of the stem within a prefabricated support structure, since such an exposure strategy requires the laser to travel through the numerous features of the support, thus defocusing the beam. Just after fabrication, the supported flower is measured to have a stem diameter of  $3.75 \pm .12 \mu\text{m}$  and a petal thickness of  $1.5 \pm 0.1 \mu\text{m}$ . Remarkably, exposure to  $\text{O}_2$  plasma for 20 min removes the supporting material, decreases the stem diameter and petal thickness to the target dimensions, and provides the flower as a freestanding structure. To verify that the final structure is in fact extremely delicate, an additional 5 min of etching is performed on an identical specimen. This additional reduction in dimensions causes the stem to buckle from electrostatic attraction between the petals and the substrate (see **Figure S4** in the Supporting Information for more details), demonstrating that the form we are able to fabricate is limited by its intrinsic properties rather than the extrinsic process limits that typically constrain design.

To summarize, we have shown that dry etching with  $\text{O}_2$  plasma allows access to an enlarged design space for structures fabricated with TPP. Structures modified by exposure to  $\text{O}_2$  plasma are shown to achieve remarkably small feature sizes. Furthermore, a strategy for inclusion of temporary support material that can be gracefully removed with plasma exposure has been shown to allow for the fabrication of exceedingly delicate structures that are geometrically complex with sub-micrometer dimensions. Critically, these techniques are immediately accessible to the growing number of researchers working with TPP, since only a slight modification in the initial device design is required and  $\text{O}_2$  plasma systems are widely available. Furthermore, since the physical processes involved for etching different materials are fundamentally similar, we anticipate that this technique can be adapted to other material chemistries through changes in process parameters, such as the chemistry of the plasma. As such, these techniques provide an avenue to realize previously inaccessible nanostructures with tailored complex geometry, thus setting the stage for future technological breakthroughs.

## Supporting Information

Supporting Information is available from the Wiley Online Library or from the author.

## Acknowledgements

This work was performed at Harvard University's Center for Nanoscale Systems (CNS), a member of the National Nanotechnology Coordinated

Infrastructure (NNCI), which is supported by the National Science Foundation under NSF award no. 1541959. Funding for this work was provided in part by Charles Stark Draper Laboratory.

## Conflict of Interest

The authors declare no conflict of interest.

## Keywords

direct laser writing, oxygen plasma, two-photon polymerization

Received: May 9, 2019

Published online: June 6, 2019

- 
- [1] M. Malinauskas, M. Farsari, A. Piskarskas, S. Juodkazis, *Phys. Rep.* **2013**, 533, 1.
- [2] J. K. Gansel, M. Thiel, M. S. Rill, M. Decker, K. Bade, V. Saile, G. von Freymann, S. Linden, M. Wegener, *Science* **2009**, 325, 1513.
- [3] T. Gissibl, S. Thiele, A. Herkommer, H. Giessen, *Nat. Photonics* **2016**, 10, 554.
- [4] H.-B. Sun, S. Matsuo, H. Misawa, *Appl. Phys. Lett.* **1999**, 74, 786.
- [5] M. Deubel, G. von Freymann, M. Wegener, S. Pereira, K. Busch, C. M. Soukoulis, *Nat. Mater.* **2004**, 3, 444.
- [6] K. K. Seet, V. Mizeikis, S. Matsuo, S. Juodkazis, H. Misawa, *Adv. Mater.* **2005**, 17, 541.
- [7] T. Ergin, N. Stenger, P. Brenner, J. B. Pendry, M. Wegener, *Science* **2010**, 328, 337.
- [8] P. Tayalia, C. R. Mendonca, T. Baldacchini, D. J. Mooney, E. Mazur, *Adv. Mater.* **2008**, 20, 4494.
- [9] T. Weiß, G. Hildebrand, R. Schade, K. Liefeth, *Eng. Life Sci.* **2009**, 9, 384.
- [10] F. Klein, T. Striebel, J. Fischer, Z. Jiang, C. M. Franz, G. von Freymann, M. Wegener, M. Bastmeyer, *Adv. Mater.* **2010**, 22, 868.
- [11] A. Doraiswamy, C. Jin, R. J. Narayan, P. Mageswaran, P. Mente, R. Modi, R. Auyeung, D. B. Chrisey, A. Ovsianikov, B. Chichkov, *Acta Biomater.* **2006**, 2, 267.
- [12] A. Ovsianikov, B. Chichkov, O. Adunka, H. Pillsbury, A. Doraiswamy, R. J. Narayan, *Appl. Surf. Sci.* **2007**, 253, 6603.
- [13] M. Medina-Sanchez, L. Schwarz, A. K. Meyer, F. Hebenstreit, O. G. Schmidt, *Nano Lett.* **2015**, 16, 555.
- [14] P. Galajda, P. Ormos, *Appl. Phys. Lett.* **2001**, 78, 249.
- [15] S. Tottori, L. Zhang, F. Qiu, K. K. Krawczyk, A. Franco-Obregón, B. J. Nelson, *Adv. Mater.* **2012**, 24, 811.
- [16] T.-Y. Huang, M. S. Sakar, A. Mao, A. J. Petruska, F. Qiu, X.-B. Chen, *Adv. Mater.* **2015**, 27, 6644.
- [17] L. R. Meza, S. Das, J. R. Greer, *Science* **2014**, 345, 1322.
- [18] X. W. Gu, J. R. Greer, *Extreme Mech. Lett.* **2015**, 2, 7.
- [19] J. Bauer, A. Schroer, R. Schwaiger, O. Kraft, *Nat. Mater.* **2016**, 15, 438.
- [20] A. Vyatskikh, S. Delalande, A. Kudo, X. Zhang, C. M. Portela, J. R. Greer, *Nat. Commun.* **2018**, 9, 593.
- [21] L. R. Meza, G. P. Philipot, C. M. Portela, A. Maggi, L. C. Montemayor, A. Comella, D. M. Kochmann, J. R. Greer, *Acta Mater.* **2017**, 140, 424.
- [22] K. Takada, H.-B. Sun, S. Kawata, *Appl. Phys. Lett.* **2005**, 86, 071122.
- [23] S. H. Park, T. W. Lim, D.-Y. Yang, R. H. Kim, K.-S. Lee, *Macromol. Res.* **2006**, 14, 559.
- [24] W. Haske, V. W. Chen, J. M. Hales, *Opt. Express* **2007**, 15, 3426.
- [25] J.-F. Xing, X.-Z. Dong, W.-Q. Chen, X.-M. Duan, N. Takeyasu, T. Tanaka, S. Kawata, *Appl. Phys. Lett.* **2007**, 90, 131106.
- [26] L. Li, R. R. Gattass, E. Gershgoren, H. Hwang, J. T. Fourkas, *Science* **2009**, 324, 910.
- [27] J. Fischer, G. von Freymann, M. Wegener, *Adv. Mater.* **2010**, 22, 3578.
- [28] S. Chizari, L. A. Shaw, J. B. Hopkins, *Mater. Horiz.* **2019**, 6, 350.
- [29] J. Fischer, M. Wegener, *Opt. Mater. Express* **2011**, 1, 614.
- [30] J. Fischer, M. Wegener, *Laser Photonics Rev.* **2013**, 7, 22.
- [31] M. M. Zieger, P. Mueller, A. S. Quick, M. Wegener, C. Barner-Kowollik, *Angew. Chem., Int. Ed.* **2017**, 56, 5625.
- [32] M. M. Zieger, P. Müller, E. Blasco, C. Petit, V. Hahn, L. Michalek, H. Mutlu, M. Wegener, C. Barner-Kowollik, *Adv. Funct. Mater.* **2018**, 28, 1801405.
- [33] D. Gräfe, A. Wickberg, M. M. Zieger, M. Wegener, E. Blasco, C. Barner-Kowollik, *Nat. Commun.* **2018**, 9, 2788.
- [34] G. Seniutinas, A. Weber, C. Padeste, I. Sakellari, M. Farsari, C. David, *Microelectron. Eng.* **2018**, 191, 25.
- [35] T. Bückmann, N. Stenger, M. Kadic, J. Kaschke, A. Frölich, T. Kennerknecht, C. Eberl, M. Thiel, M. Wegener, *Adv. Mater.* **2012**, 24, 2710.
- [36] R. Wollhofen, J. Katzmann, C. Hrelescu, J. Jacak, T. A. Klar, *Opt. Express* **2013**, 21, 10831.
- [37] S. Ramanujan, *Q. J. Math.* **1914**, 45, 350.
- [38] A. A. Bauhofer, S. Krödel, J. Rys, O. R. Bilal, A. Constantinescu, C. Daraio, *Adv. Mater.* **2017**, 29, 1703024.



## Supporting Information

for *Small*, DOI: 10.1002/sml.201902370

Additive Manufacturing of Nanostructures That Are Delicate,  
Complex, and Smaller than Ever

*Andrew J. Gross and Katia Bertoldi\**

# Supporting Information: Additive Manufacturing of Nano-Structures that are Delicate, Complex, and Smaller Than Ever

Andrew J. Gross and Katia Bertoldi

April 3, 2019

**Fabrication.** All structures in this work were fabricated using the Photonic Professional GT (Nanoscribe GmbH) tool for TPP. This system uses a laser with 780 nm wavelength, pulse width less than 100 fs, and a repetition rate of 80 MHz. The laser was focused with an inverted Zeiss microscope equipped with a Zeiss plan-apochromat 63x1.4NA Oil DIC objective lens. All structures were fabricated from the proprietary IP-Dip photoresist, which was drop cast onto silicon substrates. Some structures were fabricated primarily with piezo-rastering of the voxel, while others were fabricated primarily with galvo-scanning. For greater detail on the laser trajectories used, the code used to fabricate Lattice 2 is included as Supporting Information and the code used to fabricate the flower can be found at <http://bertoldi.seas.harvard.edu/files/bertoldi/files/flowerfabricationfiles.zip>. Development of all structures was performed by soaking in PGMEA (Baker BTS-220) for 20 minutes, then IPA (J.T. Baker) for 5 minutes, followed by super-critical CO<sub>2</sub> drying. All oxygen-plasma etching is performed at ambient temperature with 65 W power at a driving frequency of 13.56 MHz, a pressure of 760 millitorr, and 100 SCCM flow of O<sub>2</sub>. The time required to expose each structure is provided in Table S1.

| Structure                  | Exposure time<br>(minutes) |
|----------------------------|----------------------------|
| Lattice 1                  | 6                          |
| Lattice 2                  | 33                         |
| Lattice 3                  | 129                        |
| Unsupported beams          | 18                         |
| Supported beams            | 182                        |
| Unsupported flower         | 99                         |
| Partially supported flower | 195                        |
| Fully supported flower     | 318                        |

Table S1: Exposure times for the different structures fabricated.

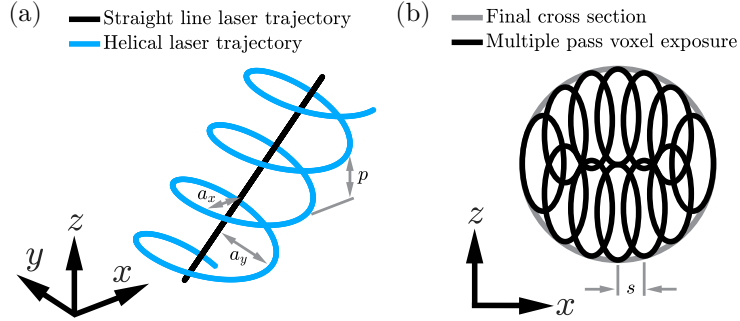


Figure S1: (a) An illustration of the different paths used to raster the voxel (i.e. the focal point of the laser illumination). The straight line laser trajectory (black) was used to fabricate Lattice 1 and the temporary support material for the beam array and flower. The helical laser trajectory (blue) was used to fabricate struts inclined to the optical axis ( $z$ -axis) in Lattices 2 and 3. The elliptical helix has periodic perturbations from the straight line trajectory in the  $x$  and  $y$  directions, with amplitudes  $a_x$  and  $a_y$ . The wavelength of periodicity is given by the pitch  $p$ , which is set to  $p = 110$  nm for all struts in Lattices 2 and 3. The amplitude of the periodic perturbations are nominally set to  $a_x = 370$  nm and  $a_y = 610$  nm. The precise values of these amplitudes were tuned to compensate for systematic variations in strut dimensions after fabrication and etching that correlated to the particular orientation of each strut. (b) An illustration of the multiple pass linear laser trajectory used to fabricate equiaxed struts that are orthogonal to the optical axis ( $z$ -axis) in Lattices 2 and 3. The gray circle is the intended cross-section and the black ellipses show the cross-section of each voxel that is superposed to achieve the intended cross-section. The horizontal placement of the ellipses are determined by the spacing  $s$ , which is nominally set to  $s = 110$  nm, while the vertical location is calculated so that the outermost extent of the voxel coincides with the surface of the intended circular cross-section. The precise location of the superposed voxels was tuned to compensate for systematic variations in strut dimensions after fabrication and etching that correlated to the particular orientation of each strut.

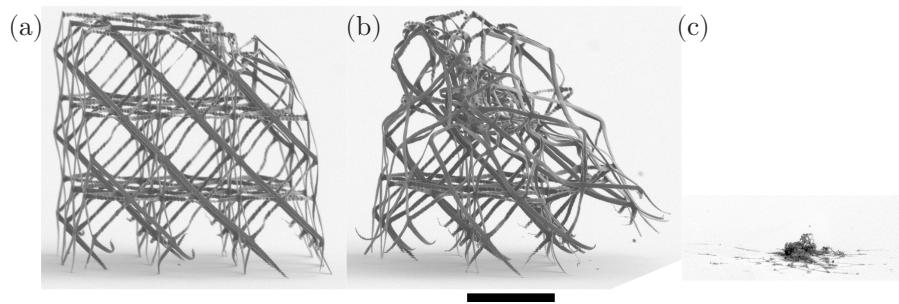


Figure S2: (a)-(b) Two micro-lattices after 11 minutes of etching. These lattices were fabricated with nearly identical parameters as Lattice 1 in Fig. 1a. The lattice in (a) is partially collapsed along one edge on its top surface, while the lattice in (b) has further collapsed, again starting from its top surface which is most accessible to the plasma. (c) After 26 minutes of etching this is what remains of the partially collapsed lattice shown in (b). The scale bar is  $10\ \mu\text{m}$ .

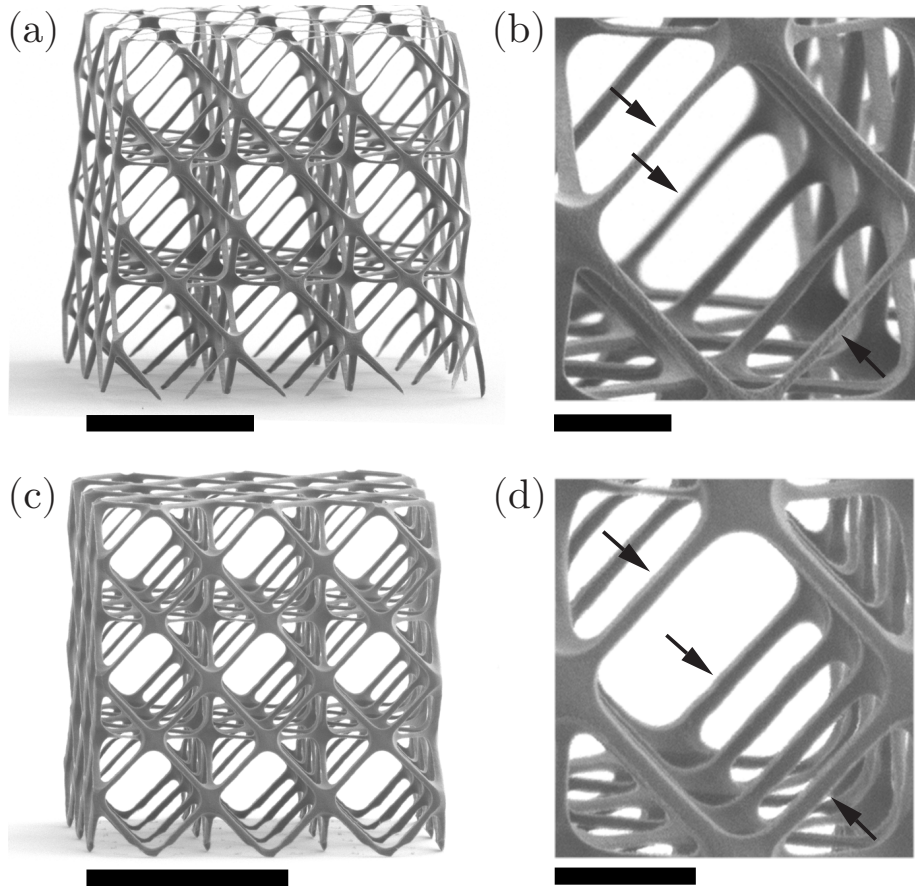


Figure S3: (a) An octahedral lattice after 35 minutes of etching. Exposure conditions for struts on the exterior of this lattice are identical to those in the interior. Due to increased access to the plasma, the exterior struts etch slightly quicker and become smaller than those on the interior after etching. This effect is strongest on the top surface of the lattice. Scale bar is  $10 \mu m$ . (b) Magnified view of the central region in lattice in (a). Exterior struts on the lateral surfaces are indicated with an arrow and are visibly smaller than struts with the same orientation in the interior. Scale bar is  $2 \mu m$ . (c) An octahedral lattice after 37.5 minutes of etching. The struts on the exterior of this lattice have been exposed with a slightly higher laser power than those in the interior (8% higher on the top surface and lateral surfaces) to compensate for their better access to the plasma. After etching the struts on the exterior are of comparable size to those in the interior. (d) Magnified view of the central region in lattice in (c). Exterior struts on the lateral surfaces are indicated with an arrow and are comparable in size to struts with the same orientation in the interior. Scale bar is  $2 \mu m$ .

| Compensation (%) | Size Difference (nm) |
|------------------|----------------------|
| 0                | 99                   |
| 2                | 89                   |
| 3                | 66                   |
| 5                | 78                   |
| 8                | -22                  |

Table S2: The results of a short process study to determine how much greater the laser power needs to be on the exterior struts in Lattice 2 so that their size after etching is the same as those throughout the interior of the lattice. Five versions of Lattice 2 were fabricated with different levels of compensation and etched for 32 minutes. The difference between the sizes of struts on the interior and exterior are reported. A negative size difference indicates that the exterior struts are larger than the interior ones after etching. Based on this study, the struts on the exterior of Lattice 2 were fabricated with a laser power 8% larger than the power of struts throughout the interior.

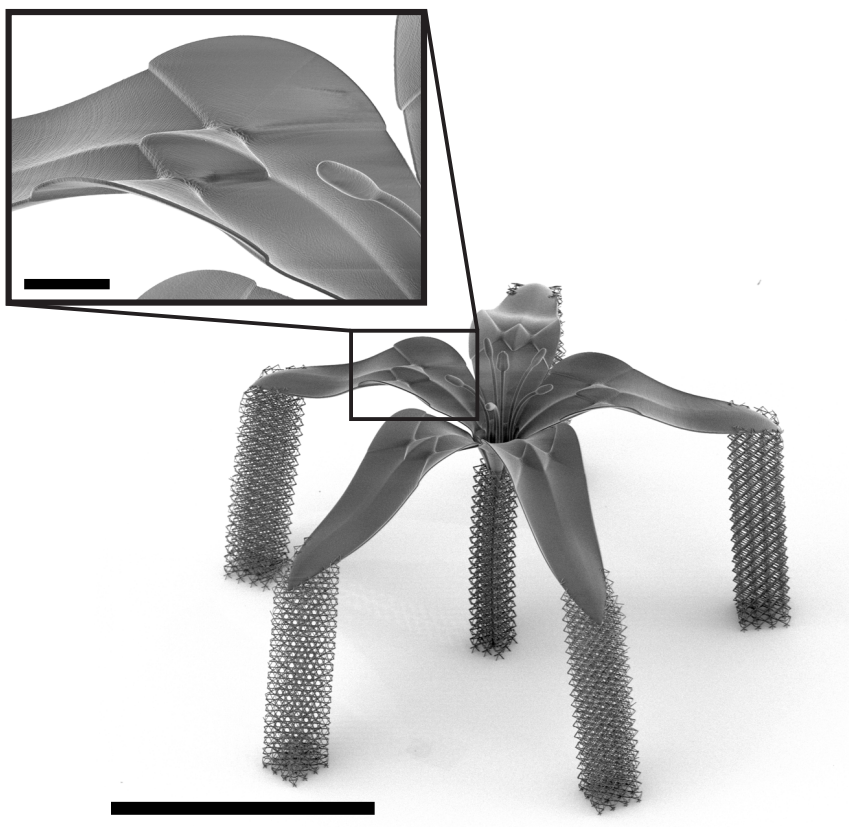


Figure S4: A flower identical to the one in Figure 4, but with only one support for each petal instead of two. The supports are sufficient to provide approximate placement of all features and prevent collapse during development, however slight bending deformation in the stem support leads to a slight misplacement of the petals. Furthermore, bending of the petal during exposure causes defective ridges (see inset image) in each petal. See Video S3 to see the details of how this defect forms. Main image scale bar is  $200\ \mu\text{m}$  and inset image scale bar is  $20\ \mu\text{m}$ .

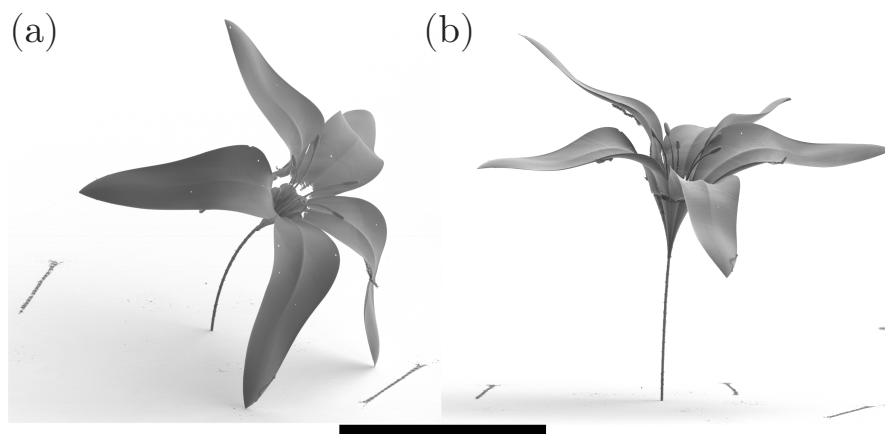


Figure S5: (a) A fully supported flower fabricated with the same parameters as that in Fig. 4 after 25 minutes of etching (5 minutes more than the flower of Fig. 4). After etching the stem diameter is reduced to  $2.7 \mu\text{m}$ , 10% smaller than the flower of Fig. 4. This slight decrease is sufficient to cause the stem to buckle under the load from electrostatic attraction between the petals and the substrate. The petals are just  $\sim 200 \text{ nm}$  thick. (b) The same flower after sputtering 10 nm of Pt/Pd to relieve electrostatic forces. With the load removed on the stem it recovers from its buckled shape. Scale bar is  $200 \mu\text{m}$ .

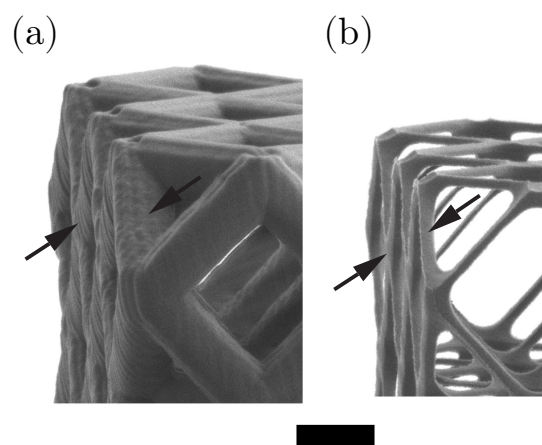


Figure S6: A close up of Lattice 2 (a) before etching and (b) after 37.5 minutes of etching. Surface roughness observed in (a) is reduced through the etching process, to the point that it is no longer perceivable in (b). Two locations on the surface before and after etching have been marked with arrows to facilitate comparison. The downwards facing arrows indicate a region on the lattice that is nearly orthogonal to the viewing direction. The upwards facing arrows indicate a region on the lattice that is imaged with near glancing incidence. The scale bar is  $2 \mu m$ .